Article

Surface Structures of SrTiO (001): A TiO-rich Reconstruction with a c(4 × 2) Unit Cell

Natasha Erdman, Oliver Warschkow, Mark Asta, Kenneth R. Poeppelmeier, Donald E. Ellis, and Laurence D. Marks

J. Am. Chem. Soc., **2003**, 125 (33), 10050-10056• DOI: 10.1021/ja034933h • Publication Date (Web): 24 July 2003

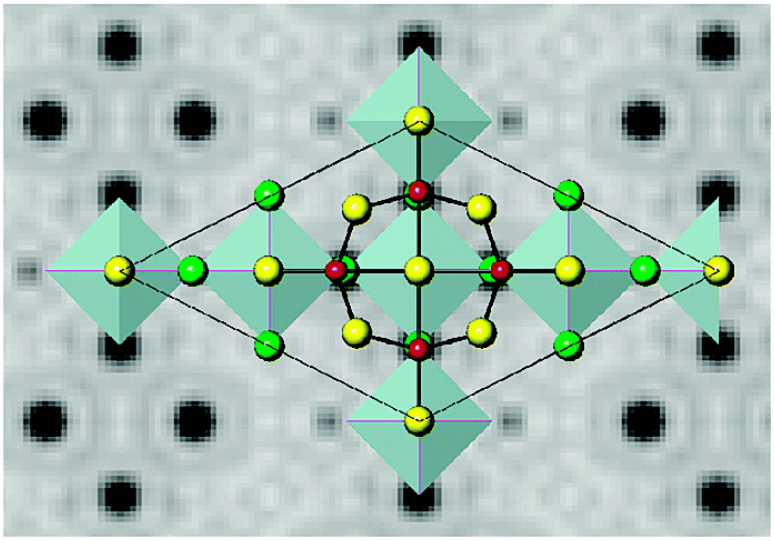

More About This Article

Additional resources and features associated with this article are available within the HTML version:

- Supporting Information
- Links to the 9 articles that cite this article, as of the time of this article download
- Access to high resolution figures
- Links to articles and content related to this article
- Copyright permission to reproduce figures and/or text from this article

View the Full Text HTML

J|A|C|S
ARTICLES
Published on Web 07/24/2003

Surface Structures of $SrTiO_3$ (001): A TiO_2-rich Reconstruction with a c(4 × 2) Unit Cell

Natasha Erdman,[†] Oliver Warschkow,[‡] Mark Asta,[§] Kenneth R. Poeppelmeier,[||] Donald E. Ellis,[‡] and Laurence D. Marks*[,†]

Contribution from the Department of Materials Science and Engineering, Institute for Environmental Catalysis, Northwestern University, Evanston, Illinois 60208-3108, Department of Chemistry, Institute for Environmental Catalysis, Northwestern University, Evanston, Illinois 60208-3108, Department of Materials Science and Engineering, Northwestern University, Evanston, Illinois 60208-3108, and Department of Physics and Astronomy, Institute for Environmental Catalysis, Northwestern University, Evanston, Illinois 60208-3108

Received February 28, 2003; E-mail: l-marks@northwestern.edu

Abstract: We report the solution of the c(4 × 2) reconstruction of $SrTiO_3$ (001), obtained through a combination of high-resolution transmission electron microscopy, direct methods analysis, and density functional theory. The structure is characterized by a single overlayer of TiO_2 stoichiometry in which TiO_5 polyhedra are arranged into edge-shared structures, in contrast to the corner-shared TiO_6 polyhedra in bulk. This structural pattern is similar to that reported by us earlier for the (2 × 1) reconstruction of the same crystal face formed at higher temperature. We discuss probable mechanisms of surface stabilization as revealed by these two solutions which are likely to apply to other reconstructions of $SrTiO_3$ (001) and, possibly, other perovskites in general.

1. Introduction

Prominent across the many disciplines of chemistry is the utility of detailed atomic structures to bring about understanding. The three-dimensional structure of a molecule, solid, or surface contains clues to a multitude of aspects, including its chemical and physical properties, the mechanism of formation, its function and utility, as well as the balance of forces that drive the atoms to arrange themselves as they are. For bulk oxides, the thousands of known crystal structures permit for an oxide of a given composition—through empirical structure rules or by analogy—the prediction of its structure. Similarly, for metal and semiconductor surfaces, enough is known from numerous resolved structures to allow structure predictions with a fair degree of confidence, facilitated perhaps by the relative short-range nature of the atomic interactions in these materials. For oxides, however, dominated by long-range Coulomb interactions, unambiguous surface structure solutions are few and far between and there is thus little in the way of empirical guidance as to how a given surface may reconstruct.[1]

Transmission electron microscopy (TEM) is a powerful technique that provides simultaneous insight into crystallographic (through diffraction) as well as morphological (bright/dark field imaging) information about a given sample. Direct methods analysis determines atom positions without the need of a trial structure by solving the phase problem intrinsically to the extent the accuracy of measured intensities permits. This yields trial structures to be subjected to both traditional structure refinement as well as geometry optimization by density functional theory (DFT). The parallel and complementary nature of this last step hopefully resolves any remaining ambiguities.

We have demonstrated this general approach recently for the (001) crystal face of $SrTiO_3$, a perovskite, with the solution of a (2 × 1) surface reconstruction.[2] Here, we report for the same crystal face, our solution of a second reconstruction with a larger c(4 × 2) unit cell.

$SrTiO_3$ is widely used technologically as a ferroelectric, thin-film substrate and buffer material.[3−5] Previous studies in recent years have tried to understand and determine surface structure variations at the (001) surface of $SrTiO_3$. Beyond the (1 × 1) bulk-terminated surface,[6] larger reconstructions with $(2 \times 1)^2$, (2 × 2),[6,7] c(4 × 2),[8−10] c(4 × 4),[9] c(6 × 2),[7,8,11] (6 × 2),[11]

* To whom correspondence should be addressed.
[†] Department of Materials Science and Engineering, Institute for Environmental Catalysis.
[‡] Department of Physics and Astronomy, Institute for Environmental Catalysis.
[§] Department of Materials Science and Engineering.
[||] Department of Chemistry, Institute for Environmental Catalysis.

(1) For an overview of the field of oxide surface science, see: (a) Freund, H. J.; Kuhlenbeck, H.; Stemmler, V. *Rep. Prog. Phys.* **1996**, *59*, 283, (b) Bonnell, D. A. *Prog. Surf. Sci.* **1998**, *57*, 187, (c) Heinrich, V. E.; Cox, P. A. *The Surface Science of Metal Oxides;* Cambridge University Press: Cambridge, 1994.
(2) Erdman, N.; Poeppelmeier, K. R.; Asta, M.; Warschkow, O.; Ellis, D. E.; Marks, L. D. *Nature* **2002**, *491*, 55.
(3) Droopad, R.; Yu, Z.; Ramdani, J.; Hilt, L.; Curless, J.; Overgaard, C.; Edwards, J. L., Jr.; Finder, J.; Eisenbeiser, K.; Ooms, W. *Mater. Sci. Eng.* **2001**, *B87*, 292.
(4) Aruta, C. *Phys. Stat. Solidi A* **2001**, *183*, 353.
(5) Jiang, Q. J.; Smilgies, D. M.; Fiedenhans'l, R.; Cardona, M.; Zegenhagen, J. *Solid State Commun.* **1996**, *98*, 157.
(6) Cord, B.; Courths, R. *Surf. Sci.* **1985**, *162*, 34.
(7) Jiang, Q. D.; Zegenhagen, J. *Surf. Sci.* **1995**, *338*, L882.

10.1021/ja034933h CCC: $25.00

$(\sqrt{5}\times\sqrt{5})$R26.6°,[10,12,13] and $(\sqrt{13}\times\sqrt{13})$R33.7°[14] unit cells have been previously observed (also, see ref 15 for a more detailed survey); yet, surface atomic structures remain undetermined for all but the $(2\times1)^2$. A number of first-principles surface structure calculations have focused on (1×1) bulklike terminations, exposing either a SrO or a TiO_2 surface layer.[16−21] We further note calculations for the larger $(2\times1)^2$ and $(\sqrt{5}\times\sqrt{5})$R26.6°[13] reconstructions.

The c(4×2) surface was previously observed by three groups:[8−10] Jiang et al.[8] prepared a c(4×2) surface by annealing of the pristine surface in hydrogen at 950 °C for 2 h. The correct periodicity was confirmed by low-energy electron diffraction (LEED). On the basis of Auger electron spectroscopy (AES) results, the authors suggested that the surface is TiO_2-terminated. The structure formation mechanism was attributed to ordering of oxygen vacancies on the surface; however, no atomic structure was proposed. A second study by Castell et al.[9] used argon ion sputtering and subsequent UHV annealing at 1200 °C for 15 min to obtain the (4×2) periodicity on the $SrTiO_3$ (001) surface. On the basis of a qualitative interpretation of STM images and LEED, the authors proposed that the surface is a bulklike TiO_2-terminated surface with several rows of Ti atoms removed such that the periodicity observed in the STM images is obtained.

In the following, we present our solution for the c(4×2) structure. We discuss the structural patterns common to both (2×1) and c(4×2) reconstructions and reflect on possible mechanisms of surface stabilization.

2. Methods

2.1. TEM and Direct Methods Analysis. In a diffraction experiment a direct Fourier inversion of the diffraction data is not possible, because while the amplitudes of the reflections are recorded, the phase information is lost. Our approach[22−25] solves the phase problem by exploiting probability relationships between the amplitudes and the phases of the diffracted beams. The algorithm searches for the set of phases with the lowest figures of merit (FOM). These approximate phases, combined with the measured amplitudes, are then used to create scattering potential maps that obey the imposed symmetry. Starting only from the intensity data, a set of plausible solutions for the structure is generated. If the experimental errors are very small or nonexistent, the peaks in such maps correlate with the actual positions of the atoms in the structure. For surface data, the intensities are more than 90% kinematical[26] (if the sample is tilted off the zone axis) and high-quality scattering potential maps can generally be obtained.

Single-crystal $SrTiO_3$ (001) wafers (99.95% pure) were cut using an ultrasonic cutter to obtain 3 mm disks, a nominal size of a TEM sample. These were mechanically polished to a thickness of about 120 μm, dimpled, and subsequently ion milled with 4.8 kV Ar^+ ions using a Gatan precision ion polishing pystem (PIPS) to produce an electron transparent sample. The sample was annealed in a tube furnace at 850−930 °C with a constant flow of high-purity oxygen to eliminate the damage caused by ion milling and to obtain the c(4×2) reconstruction. The structure is air stable and highly reproducible under the above experimental conditions. Off zone axis electron diffraction patterns, necessary for surface diffraction data analysis, and bright-field images were obtained using the UHV−H9000 Hitachi electron microscope, operated at 300 kV at Northwestern University.

A series of negatives with exposure times varying from 0.5 to 120s were recorded for the c(4×2) reconstruction using strategies that we have developed over the past decade.[27] The negatives were digitized to 8 bits with a 25 μm pixel size using an Optronics P-1000 microdensitometer. The intensities were extracted using a cross-correlation technique[28] and then averaged using a *c2mm* Patterson plane group symmetry to yield 34 independent intensities. Under the exposure conditions used, the intensity readout from the microdensitometer was proportional to the true intensities of the diffraction spots. Final structure refinement was performed based on χ^2, defined as

$$\chi^2 = 1/(N-M)\Sigma((I_{\mathrm{meas}} - I_{\mathrm{calcd}})/\sigma)^2 \qquad (1)$$

where I_{calcd} is the calculated intensity, I_{meas} the measured intensity, N the number of data points, M the number of variable parameters, and σ the measurement error.

2.2. Pseudopotential Density Functional (DFT) Calculations. The 2D nature of the diffraction data does not allow refinement of the z position; therefore, plane-wave pseudo-potential density functional calculations on a surface slab model were employed as an independent structure refinement in 3D. The surface layer with atom positions as determined by experiment was grafted onto both ends of an 11-layer slab of bulk $SrTiO_3$ (TiO_2-terminated and mirror-symmetric about a SrO layer at the center). This leads to a 13-layer model of the surface, containing 136 atoms in the primitive c(4×2) cell. Surface-slabs are separated by a slab of vacuum of approximately 12 Å thickness. During geometry optimization, all atom positions in the five surface-nearest layers were relaxed; the atom positions of the remaining three layers at the center of the slab were held frozen at bulk-positions. All calculations were performed using the ab initio total-energy and molecular-dynamics program VASP (Vienna ab initio simulation program) developed at the Institut für Materialphysik of the Universität Wien.[29−32] Specifically, Vanderbilt ultrasoft pseudopotentials[33] were used with semi-core Sr 4p and Ti 3p included as valence states in the calculation.[34] Calculations were performed within the generalized-gradient approximation (GGA) to DFT[35,36] employing a plane-wave cutoff of 337.8 eV. This combination of functional and cutoff yields a calculated formation energy of −1.23 eV for bulk $SrTiO_3$ (cubic) formed out of the binary oxides SrO and TiO_2 (rutile), which is in good agreement with the experimental value of −1.4 eV.[37] For the previous work related to the (2×1) surface[2] as well as the current calculations for the c(4×2) structures, use was made of the equivalent

(8) Jiang, Q. D.; Zegenhagen, J. *Surf. Sci.* **1999**, *425*, 343.
(9) Castell, M. R. *Surf. Sci.* **2002**, *505*, 1.
(10) Matsumoto, T.; Tanaka, H.; Kawai, T.; Kawai, S. *Surf. Sci.* **1994**, *318*, 29.
(11) Castell, M. *Surf. Sci.* **2002**, *516*, 33.
(12) Martin-Gonzalez, M. S.; Aguirre, M. H.; Morgan, E.; Alario-Franco, M. A.; Perez-Dieste, V.; Avila, J.; Asensio, M. C. *Solid State Sci.* **2000**, *2*, 519.
(13) Kubo, T.; Nozoye, H. *Phys. Rev. Lett.* **2001**, *86*, 1801.
(14) Naito, M.; Sato, H. *Physica C* **1994**, *229*, 1.
(15) Erdman, N.; Marks, L. D. *Surf. Sci.* **2003**, *526*, 107.
(16) Padilla, J.; Vanderbilt, D. *Phys. Rev. B* **1997**, *56*, 1625.
(17) Padilla, J.; Vanderbilt, D. *Surf. Sci.* **1998**, *418*, 64.
(18) Meyer, B.; Padilla, J.; Vanderbilt, D. *Faraday Discuss.* **1999**, *114*, 395.
(19) Cheng, C.; Kunc, K.; Lee, M. H. *Phys. Rev. B* **2000**, *62*, 10409.
(20) Heifets, E.; Eglitis, R. I.; Kotomin, E. A.; Maier, J.; Borstel, G. *Phys. Rev. B* **2001**, *64*, 235417.
(21) Heifets, E.; Eglitis, R. I.; Kotomin, E. A.; Maier, J.; Borstel, G. *Surf. Sci.* **2002**, *513*, 211.
(22) Marks, L. D.; Grozea, D.; Feidenhans'l, R.; Nielsen, M.; Johnson, R. L. *Surf. Rev. Lett.* **1998**, *5*, 1087.
(23) Marks, L. D.; Erdman, N.; Subramanian, A. *J. Phys.: Condens. Matter* **2001**, *13*, 10677.
(24) Collazo-Davila, C.; Grozea, D.; Marks, L. D. *Phys. Rev. Lett.* **1998**, *80*, 1678.
(25) Marks, L. D.; Sinkler, W.; Landree, E. *Acta Crystallogr.* **1999**, *55*, 601.
(26) Xu, P.; Marks, L. D. *Ultramicroscopy* **1992**, *45*, 155.
(27) Jayaram, G.; Xu, P.; Marks, L. D. *Phys. Rev. Lett.* **1993**, *71*, 3489.
(28) Xu, P.; Jayaram, G.; Marks, L. D. *Ultramicroscopy* **1994**, *53*, 15.
(29) Kresse, G.; Hafner, J. *Phys. Rev. B* **1993**, *47*, 558.
(30) Kresse, G.; Hafner, J. *Phys. Rev. B* **1994**, *49*, 14251.
(31) Kresse, G.; Furthmüller, J. *Comput. Mater. Sci.* **1996**, *6*, 15.
(32) Kresse, G.; Furthmüller, J. *Phys. Rev. B* **1996**, *54*, 11169.
(33) Vanderbilt, D. *Phys. Rev. B* **1990**, *41*, 7892.
(34) Kresse, G.; Hafner, J. *J. Phys.: Condens. Matt.* **1994**, *6*, 8245.
(35) Perdew, J. P. In *Electronic Structure of Solids '91*; Ziesche, P., Eschrig, H., Eds.; Akademie Verlag: Berlin, 1991; p 11.
(36) Perdew, J. P. Chevary, J. A.; Vosko, S. H.; Jackson, K. A.; Pederson, M. R.; Singh, D. J.; Fiolhais, C. *Phys. Rev. B* **1992**, *46*, 6671.
(37) Takayama-Muromachi, E.; Navrotsky, A. *J. Solid State Chem.* **1988**, *72*, 244.

k-point method proposed by Froyen.[38] This method ensures strict equivalence of *k*-point grids employed in reciprocal space integrations performed for each of the surface unit cells considered. In all of the calculations reported here and in ref 2, the *k*-point mesh was taken equivalent to 4 × 4 × 1 for the full (reducible) Brillouin zone corresponding to a reference 1 × 1 surface-unit cell. This is particularly relevant when the slab energies of different reconstructions are to be compared. We note in this context that, generally, in the calculation of absolute surfaces energies as well as energy differences between two reconstructions, stoichiometry differences between surface/bulk and surface/surface, respectively, have to be accounted for via suitable chemical potentials (e.g., TiO_2, SrO, and O_2). If two reconstructions have the same stoichiometry, the surface energy difference is independent from these chemical potentials. All energy comparisons reported in the following text are of this type.

2.3. LCAO-DFT Calculations. Seeking a qualitative perspective on charge transfer and bonding, local densities of states (LDOS), partial atomic charges, and populations were calculated using a separate linear combination of atomic orbital (LCAO) model. Here, the DFT equations were solved in the local density approximation (LDA, $X\alpha = 0.7$ scaled exchange functional[39]) in the framework of the discrete-variational (DV) method.[40−42] Owing to the size of the system, a linear-scaling divide-and-conquer (DAC) ansatz was employed[43−45] in which every symmetry-unique atom is described by a local cluster of atoms embedded into the effective Kohn−Sham potential of all the other atoms of the slab. A near minimal LCAO basis set of numerical atomic orbitals has been used in the calculations. The Ti and Sr cation basis sets includes atomic orbitals up to 4p and 5p, respectively. The oxide basis set is of a double-valence type containing two sets of 2s and 2p orbitals to increase variational flexibility. DAC clusters were generated by adding to the atom defined by the cluster all atoms within a radius of 9 au for O- and Ti− defining clusters and 10.5 au for Sr-defining clusters as "buffer atoms".[44,45] With this cutoff, Sr, Ti, and O atoms in bulk $SrTiO_3$ are described using clusters of 45, 63, and 29 atoms, respectively. Clusters describing surface-near atoms contain fewer atoms. All reported partial charges were computed using Mulliken-type partitioning of electron densities.

3. Results

Figure 1 shows an off-zone axis selected area diffraction pattern with both 4 × 2 and 2 × 4 domains (the primitive cells are marked on the figure) combined with a bright-field image of the $SrTiO_3$ (001) sample. The bright-field image indicates the formation of large flat ⟨100⟩ facets (50−200 nm wide) on the surface of the sample following annealing. The small rectangular features ∼2−10 nm in size are attributed to formation of voids in the near surface region.[15] Whereas the majority of the step edges are oriented along [100] or [010] directions, in some areas it can be clearly seen that ⟨110⟩ type facets are stabilized as a result of annealing.

Figure 2a shows the c(4 × 2) structure solution obtained through direct methods in terms of a scattering potential map. The map shows the dominant structural motif, a block of four features. Analysis indicated that these features were Ti atom sites (not O or Sr), and using conventional difference maps combined with χ^2 refinements we were able to determine the oxygen atom positions in the top layer. The refinement of the top layer structure against the diffraction data gave both the Ti and O atom positions with a $\chi^2 = 2.1$. Figure 2b shows the interpretation of the scattering potential map in terms of TiO_x pseudo-octahedral units. Alternative models of the structure were

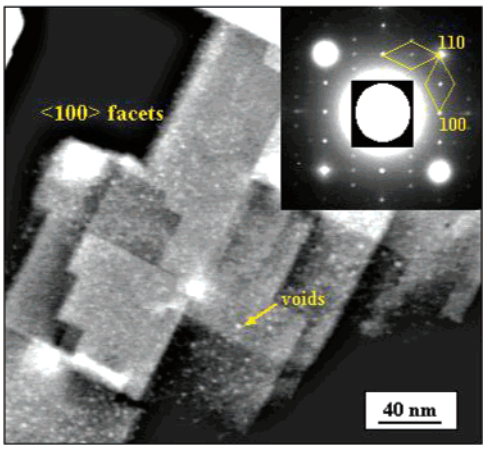

Figure 1. Off-zone axis diffraction pattern with both (4 × 2) and (2 × 4) domains (the primitive cells are marked on the figure) combined with a bright-field image of the $SrTiO_3$ (001) sample.

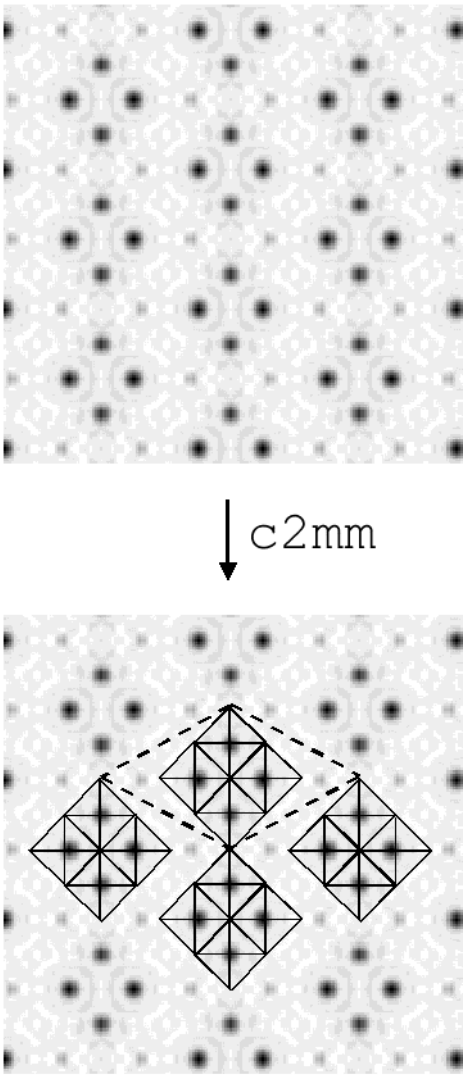

Figure 2. (a) Scattering potential obtained through direct methods analysis. The dark features were determined to be Ti atom sites. (b) Interpretation of the scattering potential map in terms of TiO_x pseudo-octahedral units.

(38) Froyen, S. *Phys. Rev. B* **1989**, *39*, 3168.
(39) Slater, J. C.; Wilson, T. M.; Wood, J. H. *Phys. Rev.* **1969**, *179*, 28.
(40) Ellis, D. E.; Painter, G. S. *Phys. Rev. B* **1970**, *2*, 2887.
(41) Baerends, E. J.; Ellis, D. E.; Ros, P. *J. Chem. Phys.* **1973**, *2*, 41.
(42) Rosen, A.; Ellis, D. E.; Adachi, H.; Averill, F. W. *J. Chem. Phys.* **1976**, *65*, 3629.
(43) Yang, W. Phys. *Rev. Lett.* **1991**, *66*, 1438.
(44) Yang, W.; Lee, T. S. *J. Chem. Phys.* **1995**, *103*, 5674.
(45) Warschkow, O.; Dyke, J. M.; Ellis, D. E. *J. Comput. Phys.* **1998**, *143*, 70.

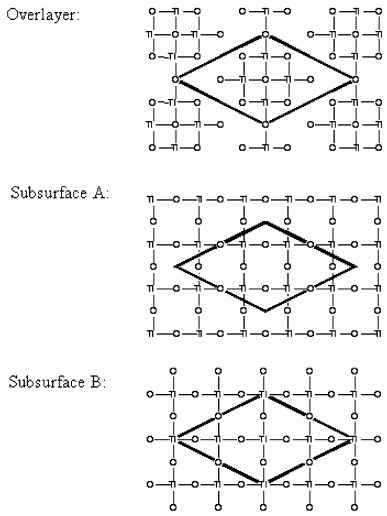

Figure 3. Schematic diagram illustrating the two possible registries of the c(4 × 2) overlayer with the TiO_2 layer of bulk $SrTiO_3$ underneath (the subsurface), leading to the A and B structures discussed in the text.

considered, differing in type and stoichiometry of the subsurface layer, its relative position with respect to the top layer, as well as addition of O on top of the Ti atoms; however, the refinement results were significantly inferior to the proposed solution. Specifically, the refinement showed that subsurface layer is of TiO_2 and not of SrO stoichiometry.

The *x*,*y* positions of atoms in the top layer of the structure were deduced quite unambiguously from the scattering potential maps. These positions indicate that the surface structure consists of a combination of edge sharing TiO_x units with four Ti atoms in each unit. The manner in which this surface layer could attach to the underlying bulk layers, however, presented some ambiguity. Bearing in mind the coordination requirements for perovskite and ReO_3-type structures as well as the 2 × 1 surface structure reported previously,[2] we considered two possible configurations of the overlayer with respect to the bulk, schematically illustrated in Figure 3.

Hereafter, for simplicity, we will refer to the structures as A and B. Additional electron diffraction data refinements were performed using these two possible configurations of the subsurface layer with respect to the surface TiO_x overlayer. The refinement yielded a better fit for structure B ($\chi^2 = 1.9$) than for structure A ($\chi^2 = 2.4$). Separate from the experimental refinement, structures for the A and B surface were obtained through DFT geometry optimization and are displayed in Figures 4 and 5. The experimental and DFT-calculated atomic positions for both A and B structures are summarized in Tables 1 and 2, respectively.

Because we find calculated *x*,*y* atomic positions of both A and B surfaces to be consistent with both experimental positions, an assignment of the observed structure can be made based on the calculated surface energies. The DFT calculations reveal the B surface structure to be substantially more stable relative to the A surface by 0.53 J/m^2 (or 33 meV/Å^2). The A structure, incidentally, has a very similar surface energy ($\Delta E < 0.05$ J/m^2) to our (2 × 1) reconstruction;[2] thus, the B-type c(4 × 2) is also more stable with respect to the (2 × 1) structure that is experimentally observed at higher temperatures.[2,15] Together, better refinement result and a lower surface energy strongly

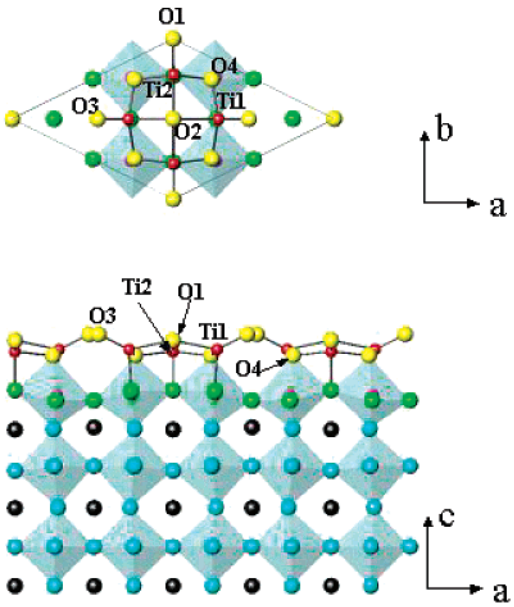

Figure 4. Top and side view of the relaxed c(4 × 2) with the high-energy type-A registry with the underlying bulk.

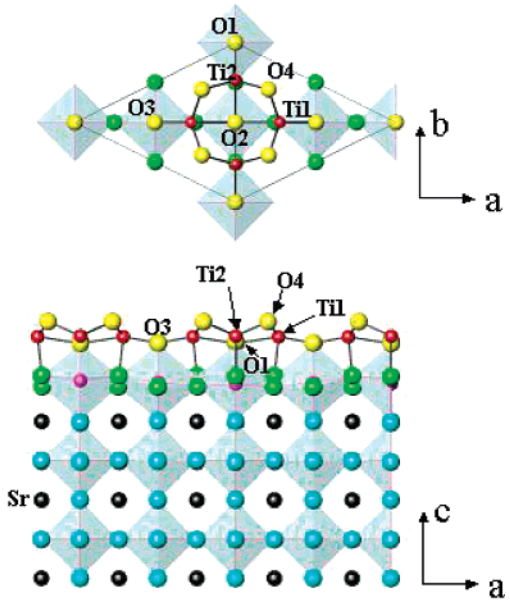

Figure 5. Top and side view of the relaxed c(4 × 2) with the low-energy type-B registry with the underlying bulk.

suggest that the observed c(4 × 2) surface has the B-type structure.

Selected bond distances in the surface layer of the type-B c(4 × 2) reconstruction are listed in Table 3. Partial atomic charges for surface-near atoms, calculated using both a first-principles LCAO-DFT model and an empirical bond-valence-model,[46] are provided in Table 4. We point out that Mulliken-partitioned DFT charges should only be interpreted in relative terms; thus, the calculated +1.99 charge represents the reference for a Ti atom of formal charge +IV. The DFT near-surface charges for Ti atoms exhibit only small changes with respect to bulk Ti (+1.88 and +1.95 vs +1.99), suggesting that they are well described as Ti(IV) species; this is confirmed by bond-valence model, which yields charges close to four for these

(46) Brese, N. E.; O'Keeffe, M. *Acta Crystallogr. B* **1991**, *47*, 192.

Table 1. Experimental and DFT Atom Positions for the Low-Energy c(4 × 2) Type B Reconstruction of $SrTiO_3$ (001)[a]

layer	atom	X	Y	Z (Å)	$\lvert Z_{bulk} - Z_{DFT}\rvert$ (Å)
1 (overlayer)	Ti1	0.3622	0	12.168	0.453
		0.3761			
	Ti2	1/2	0.2625	12.208	0.493
			0.2461		
	O1	0	0	11.940	0.225
	O2	1/2	0	11.848	0.133
	O3	0.2488	0	11.828	0.113
		0.2455			
	O4	0.3962	0.2064	12.932	1.217
		0.3771	*0.2077*		
2 (subsurface)	Ti21	0	0	9.794	0.032
	Ti22	1/2	0	9.859	0.097
	Ti23	0.2405	0	9.969	0.207
	O21	1/4	1/4	9.640	0.123
	O22	0.1227	0	9.633	0.130
	O23	1/2	0.2529	10.203	0.441
	O24	0.3756	0	10.179	0.417
3	Sr	0.3682	0.2514	7.895	0.085
	O	0	0	7.918	0.108
	O	1/2	0	8.019	0.209
	O	0.2585	0	7.835	0.025

[a] Listed are positions obtained from χ^2 refinement (in italics font) as well as DFT geometry optimization. In the table, *x* and *y* positions are given in fractional coordinates for a rectangular cell ($a = 15.62$ Å, $b = 7.810$ Å, *c*2*mm)*. The *z* coordinate is in Å with respect to the center-most layer of the slab model.

Table 2. DFT Atom Positions for the High-Energy Type A Structure of the c(4 × 2) Reconstruction[a]

layer	atom	X	Y	Z (Å)	$\lvert Z_{bulk} - Z_{DFT}\rvert$ (Å)
1 (overlayer)	Ti1	0.3607	0	12.025	0.310
	Ti2	1/2	0.2757	11.917	0.202
	O1	0	0	12.458	0.743
	O2	1/2	0	12.480	0.765
	O3	0.2653	0	12.768	1.053
	O4	0.3800	0.2465	11.728	0.013
2 (subsurface)	Ti21	0.3678	0.2608	9.788	0.026
	O21	1/4	1/4	9.507	0.256
	O22	0.1294	0	9.515	0.248
	O23	1/2	0.2686	10.018	0.256
	O24	0.3676	0	9.975	0.213
3	Sr	0	0	7.821	0.011
	Sr	1/2	0	7.933	0.123
	Sr	0.2562	0	7.819	0.009
	O	0.3872	0.2289	7.859	0.049

[a] In the table, *x* and *y* positions are given in fractional coordinates for a rectangular cell ($a = 15.62$ Å, $b = 7.810$ Å, *c*2*mm*). The *z* coordinate is given in Å with respect to the center-most layer of the slab model.

atoms. This assignment of the Ti charge state is overall consistent with the stoichiometry of the surface as nonreduced and TiO_2-rich (i.e., $SrTiO_3 + xTiO_2$). The surface charges for oxygen atoms calculated by the DFT model are paralleled by the bond-valence model charges. In particular, the 5-fold coordinated oxygen atom at the center (O2) is clearly the most highly ionic; in contrast, the two types of 2-fold angled coordinated oxygen atoms, O3 and O4, have lower charges, clearly smaller than O2 but also somewhat reduced with respect to bulk oxygen.

4. Discussion

The structure of $SrTiO_3$ along the [001] direction can be described in terms of alternating layers with SrO and TiO_2 stoichiometry stacked together such that Ti and O form a network of corner-shared TiO_6 octahedra. Simple termination of this stacking sequence at a TiO_2 layer results in a $SrTiO_3$ (001) surface characterized by truncated, corner-sharing octahedra in the surface layer. In these truncated octahedra, Ti is undercoordinated, having only five nearest oxygen atoms (four in plane, one below). Because corner-shared octahedra are highly interconnected, there is little flexibility to permit atomic relaxation into 5-fold coordination geometries that are perhaps more favorable than that of a truncated octahedron. Since undercoordinated Ti is hardly avoidable near any surface, it may well be that it is the ability to locally stabilize undercoordinated Ti sites that decides the relative stability of competing reconstructions.

Table 3. Comparison of Bond Distances to Nearest Neighbors of Ti1 and Ti2 Sites in the Overlayers of the c(4 × 2) (A and B structures) Reconstructions of $SrTiO_3$ (001)[a]

		distance/Å	
site		c(4×2) B	c(4×2) A
Ti1	O2 (1×)	2.18	2.22*
	O3 (1×)	1.80	1.67*
	O4 (2×)	1.86*	1.97
	O24 (1×)	2.00	2.05
Ti2	O1 (1×)	1.87	1.83*
	O2 (1×)	2.08	2.23*
	O4 (2×)	1.83*	1.90
	O23 (1×)	2.01	1.90

[a] O22 and O24 are oxygen atoms in the subsurface layer. Floating oxygen sites are marked with an asterisk (*).

Table 4. Partial Atomic Charges for Surface Atoms of the c(4 × 2) B Structure[a]

layer	site	Mulliken charge/e	bond valence charge/e	coordination number
1 (overlayer)	Ti1	+1.88	+3.78	5
	Ti2	+1.95	+3.86	5
	O1	−1.03	−2.11	3
	O2	−1.21	−2.35	5
	O3	−0.84	−1.91	2
	O4	−0.86	−1.85	2
2 (subsurface)	Ti21	+2.01	+4.05	6
	Ti22	+1.97	+4.08	6
	Ti23	+2.01	+3.84	6
	O21	−1.16	−1.90	4 (2Ti, 2Sr)
	O22	−1.12	−2.14	4 (2Ti, 2Sr)
	O23	−1.11	−1.99	5 (3Ti, 2Sr)
	O24	−1.13	−1.88	5 (3Ti, 2Sr)
bulk ($SrTiO_3$ cubic)	Ti	+1.99	+4.14	6
	Sr	−1.54	+2.11	12
	O	−1.17	−2.08	6 (2Ti, 4Sr)

[a] Charges were calculated using (a) Mulliken partitioning of the electron density obtained by a LCAO-DFT model; (b) bond-valence model applied to the energy minimized geometry (Table 1).

From our solution of the c(4 × 2) and the earlier reported (2 × 1),[2] we learn that such stabilization can be accomplished by means of an additional TiO_2 overlayer placed on top of the bulklike TiO_2 layer (henceforth referred to as the "subsurface layer"). In both reconstructions we observe the following:

(1) TiO_2 stoichiometry in the overlayer and the subsurface layer; all ions retain their formal oxidation states.

(2) The propensity in the overlayer toward arranging 5-fold coordinated Ti into edge-shared polyhedra in contrast to the corner-shared arrangement in the subsurface layer below and the bulk at large.

(3) No vacancies in the overlayer, i.e., the overlayer contains the same number of atoms as the subsurface or a bulklike TiO_2 layer. We refer to this quality in the following as "maximum occupancy"; we can rationalize it if we expect Ti in the overlayer

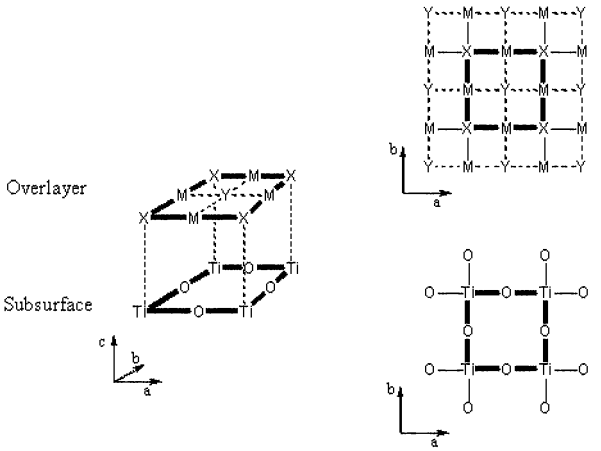

Figure 6. Schematic of possible cation and anion sites in the formation of a TiO_2 stoichiometric overlayer on $SrTiO_3$ (001). Sites X and Y denote "structural" and "floating" oxygen sites, respectively (cf. text). M denotes possible Ti sites. In the c(4 × 2) and (2 × 1) structure, all anion sites (X and Y) and one-half of the Ti sites are occupied.

to be at least five-coordinated, which necessitates the tight packing of TiO_5 units.

We believe there exists a common mechanism which drives the c(4 × 2) and (2 × 1) structures to reconstruct in this particular way, and with knowledge of the specific atom arrangements in the surface layer through solution of the c(4 × 2) surface structure presented in this paper, we should be able to shed some light on it. The understanding of this mechanism would yield empirical rules to help elucidate the structuring and formation of other related surfaces, applicable not only to $SrTiO_3$ but, quite possibly, to perovskites in general.

In the formation of the overlayer, the TiO_2 subsurface layer is clearly the strongest determinant in the precise placement of atoms in the overlayer, acting in many respects as a template. We consider three types of possible atomic sites in the overlayer, two types for oxygen and one for titanium (Figure 6).

(1) "Coordinating" oxygen sites (site X in Figure 6) are positioned directly above Ti atoms in the subsurface layer, providing the missing sixth coordinator. In our 'constructionists' rationalization of overlayer formation, we consider this to be its driving force, as this stabilizes the otherwise unfavorable corner-shared TiO_5 truncated octahedra in the subsurface. For every (1 × 1) surface unit there is one site of this type.

(2) Considering the length of a typical Ti−O bond, the only reasonable location for Ti atoms in the overlayer is between two "coordinating" oxygen sites (site M in Figure 6). This further places it above another oxygen atom in the subsurface. There are two sites of this type for every (1 × 1) surface unit.

(3) We would expect Ti to require five coordinating oxygen atoms at least. This warrants a second type of oxygen site in the overlayer, located at the center of each (1 × 1) cell (site Y in Figure 6). We refer to this casually as a "floating" oxygen site, because it is has no atom located directly underneath in the subsurface layer. This characterizes this site with a fair degree of positional flexibility in the vertical direction. Note that an oxygen atom at this site requires at least one of the four adjacent Ti sites to be occupied. Of this type of oxygen, there is one per (1 × 1) surface unit.

This list serves as a catalog of possible sites in a single overlayer, not all of which must necessarily be occupied. Both the $(2 \times 1)^2$ and the c(4 × 2) (including the alternative A structure) are fully described in these terms. With two cation and two anion sites per (1 × 1) surface unit, the maximum number of TiO_2 units is limited by the number of oxygen sites: such an overlayer has all oxygen sites ("coordinating" X as well as "floating" Y) occupied together with one-half of all cation sites M. Thus, in a TiO_2 stoichiometric overlayer of maximum occupancy, the principle variable is how Ti atoms are distributed over twice as many cation sites. The (2 × 1) and c(4 × 2) solution (B structure) as well as the higher energy A structure of the c(4 × 2) present three distinct distribution patterns. Other patterns are conceivable and may indeed describe other observable reconstructions. Clearly, certain Ti distributions are more favorable than others, and the (2 × 1) and c(4 × 2) structures should help us identify some of the stabilizing principles.

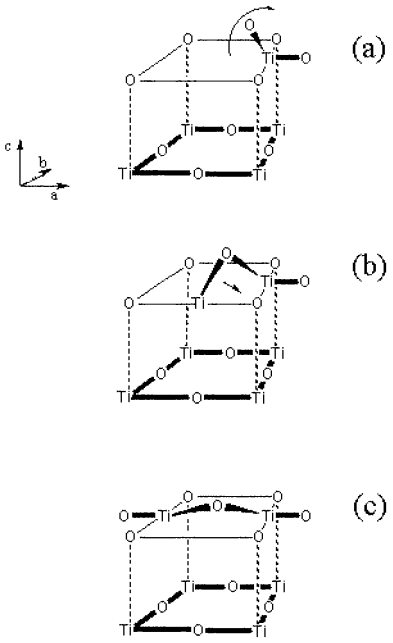

Figure 7. "Floating" oxygen sites in the $SrTiO_3$ (001) overlayer, not bound to Ti in the subsurface layer below, are characterized by varying degrees of flexibility depending on how many and which of the four adjacent Ti sites are occupied. In single coordination (a) and 2-fold cis-coordination (b), the oxygen atom can displace out of the surface plane without stretching Ti−O bonds. Two-fold trans-coordinated oxygen atoms (c), as well as 3- and 4-fold coordinated oxygen (not displayed) are rigidly bound; significant out of plane displacements cannot occur without Ti−O bond stretching.

As indicated above, structural flexibility in this type of reconstruction is largely provided by the type Y "floating" oxygens in the overlayer; however, the degree of flexibility at this site is very dependent on which and how many of the nearest in-layer cation sites are occupied (Figure 7). With only one of the four cation sites occupied, that is, the O bound to only one Ti atom, its positional flexibility is at a maximum; as found, for example, in the $(2 \times 1)^2$ and the A-type c(4 × 2) (O3 in Figure 4), the single-bound oxygen arcs out of the surface layer, resulting in a near bipyramidal coordination for the Ti atom. Floating oxygen coordinated by two Ti atoms can be distinguished into two variants: linear (cis) and angled (trans) depending on the relative positioning of the two coordinating Ti atoms in the four cation sites (Figure 7). Critical for positional flexibility of the oxygen atom is that 2-fold cis-coordinated oxygen can swing out of the surface layer (arcing into ⟨110⟩ direction) without having to lengthen the Ti−O bond lengths; for the 2-fold trans- as well as for 3- and 4-fold coordinated

oxygen atoms, any displacement out of the surface layer necessitates Ti−O bond lengthening. Thus, if indeed out-of-plane displacements of floating oxygen atoms are a significant source of surface stabilization, then we would expect particularly stable reconstructions to be characterized by a Ti atom distribution such that it contains a maximum of single-coordinated and 2-fold cis-coordinated floating oxygen atoms.

Qualitatively, the A and B structure of the c(4 × 2) differ in that "coordinating" and "floating" oxygen sites are interchanged. The shift of the underlying bulk between A and B structures causes oxygen atoms that are "coordinating" in the A structure to become "floating" in the B and visa versa. A and B surface thus differ significantly in how the positional flexibility provided by the floating oxygen atoms is allocated over the surface: In the B structure, all four floating oxygen sites (O4, Figure 5) are 2-fold cis-coordinated and therefore capable of flexing out of the plane of the overlayer. In the A structure, two of the four floating oxygen atoms are of the flexible 1-fold coordinated type (O3, Figure 4), the other two are 2-fold linear coordinated (O1), thus of limited flexibility. Of the two floating oxygen atoms in the (2 × 1) reconstruction,[2] one is 1-fold coordinated flexible and the other is 3-fold coordinated nonflexible. In summary, the c(4 × 2) B structure is characterized by positional flexibility in one-half of its oxygen atoms in the overlayer (i.e., all floating oxygen atoms); both the c(4 × 2) A structure and the (2 × 1) have this flexibility in only one-quarter of overlayer oxygen atoms. This correlates well with our finding that the calculated surface energies of c(4 × 2) structure A and the (2 × 1) are very similar and significantly higher than of the c(4 × 2) B-structure.

In all structures, c(4 × 2) (A and B structure) as well as (2 × 1),[2] we further observe that subsurface oxygen atoms which are bound to Ti atoms in the overlayer exhibit a small vertical displacement out of the subsurface layer toward the surface. In contrast, oxygen atoms not bound to overlayer Ti atoms are displaced away from the surface. In the case of the A-type c(4 × 2) and the (2 × 1), this displacement of oxygen atoms leads to a regular tilting of subsurface TiO_6 octahedra; the octahedra are tipped sequentially in the (100) and (−100) direction, reminiscent of the distortion observed in low-temperature noncubic perovskite phases. In contrast, the more stable B reconstruction (Figure 5) exhibits an irregular distortion of subsurface TiO_6 octahedra. This suggests that it is the overlayer structure which determines how subsurface TiO_6 octahedra tilt or otherwise distort.

5. Conclusions

We report the solution of c(4 × 2) reconstruction of $SrTiO_3$ (001) based on high-resolution transmission electron microscopy and direct methods analysis. Plane-wave pseudo-potential calculations confirmed the registry of the surface layer with the bulk and provided the *z* positions of the structure. As found for the (2 × 1) reconstruction,[2] the c(4 × 2) surface is characterized by a single TiO_2 overlayer in which Ti atoms are arranged into edge-shared truncated octahedra. We propose that the distribution of Ti atoms in the overlayer is determined such that a maximum of vertical positional flexibility is realized for those overlayer oxygen atoms not bound to the subsurface; it is this flexibility that permits 5-fold coordinated Ti atoms in the surface later to stabilize away from an unfavorable truncated octahedral coordination.

Acknowledgment. This work was supported by the EMSI program of the National Science Foundation and the U.S. Department of Energy Office of Science (CHE-9810378) at the Northwestern University Institute for Environmental Catalysis. Research of M.A. was supported by the NSF under program DMR-0076063.

JA034933H